Selected for a Viewpoint in *Physics*

RAPID COMMUNICATIONS

PHYSICAL REVIEW B **81**, 041402(R) (2010)

Spontaneous inversion symmetry breaking in graphene bilayers

Fan Zhang,[1] Hongki Min,[1] Marco Polini,[2] and A. H. MacDonald[1]

[1]*Department of Physics, University of Texas at Austin, Austin, Texas 78712, USA*

[2]*NEST-CNR-INFM and Scuola Normale Superiore, I-56126 Pisa, Italy*

(Received 30 July 2009; revised manuscript received 4 November 2009; published 4 January 2010)

In a mean-field-theory treatment the ground state of a graphene bilayer spontaneously breaks inversion symmetry for arbitrarily weak electron-electron interactions when trigonal-warping terms in the band structure are ignored. We report on a perturbative renormalization-group calculation, which assesses the robustness of this instability, comparing with the closely related case of the charge-density-wave instability incorrectly predicted by mean-field theory in a one-dimensional electron gas. We conclude that spontaneous inversion symmetry breaking in graphene is not suppressed by quantum fluctuations but that, because of trigonal warping, it may occur only in high quality suspended bilayers.

DOI: 10.1103/PhysRevB.81.041402 PACS number(s): 71.10.Hf, 71.10.Pm

Electrons most often organize into Fermi-liquid states in which interactions play an inessential role. A well-known exception is the case of one-dimensional (1D) electron systems (1DESs). In 1D, the electron Fermi surface consists of points, and divergences associated with low-energy particle-hole excitations abound when electron-electron interactions are described perturbatively. In higher space dimensions, the corresponding divergences occur only when Fermi lines or surfaces satisfy idealized nesting conditions. In this article we discuss electron-electron interactions in two-dimensional (2D) graphene bilayer systems, which behave in many ways as if they were one dimensional because they have Fermi points instead of Fermi lines and because their particle-hole energies have a quadratic dispersion which compensates for the difference between 1D and 2D phase space.

Recent progress in the isolation of nearly perfect single and multilayer graphene sheets[1–4] has opened up a new topic in two-dimensional electron systems (2DESs) physics. There is to date little unambiguous experimental evidence that electron-electron interactions play an essential role in the graphene family of 2DESs. However, as pointed out by Min *et al.*[5] graphene bilayers near neutrality should be particularly susceptible to interaction effects because of their peculiar massive-chiral[6] band Hamiltonian, which has an energy splitting between valence and conduction bands that vanishes at $\boldsymbol{k}=\mathbf{0}$ and grows quadratically with $k=|\boldsymbol{k}|$,

$$\mathcal{H}_B = -\sum_{k\sigma'\sigma} \frac{\hbar^2 k^2}{2m^*} c^\dagger_{k\sigma'} [\cos(J\phi_{\boldsymbol{k}})\tau^x_{\sigma'\sigma} + \sin(J\phi_{\boldsymbol{k}})\tau^y_{\sigma'\sigma}] c_{k\sigma}. \tag{1}$$

In Eq. (1) the τ^is are Pauli matrices and the Greek labels refer to the two bilayer graphene sublattice sites, one in each layer, which do not have a neighbor in the opposite graphene layer (see Fig. 1.) The other two sublattice site energies are repelled from the Fermi level by interlayer hopping and irrelevant at low energies. It is frequently useful to view quantum two-level layer degree of freedom as a pseudospin. The $J=2$ pseudospin chirality of bilayer graphene contrasts with the $J=1$ chirality[1,7] of single-layer graphene and is a consequence of the two-step process in which electrons hop between low-energy sites via the high-energy sites. The massive-chiral band-structure model applies at energies smaller than the interlayer hopping scale[4] $\gamma_1 \sim 0.3$ eV but larger than the trigonal-warping scale[4] $\gamma_3\gamma_1/\gamma_0 \sim 0.03$ eV below which direct hopping between low-energy sites plays an essential role. The body of this Rapid Communication concerns the role of interactions in the massive-chiral model; we return at the end to explain the important role played by trigonal warping.

Similarities and differences between graphene bilayers and 1DES are most easily explained by temporarily neglecting the spin, and in the case of graphene also the additional valley degree of freedom. As illustrated in Fig. 1 in both

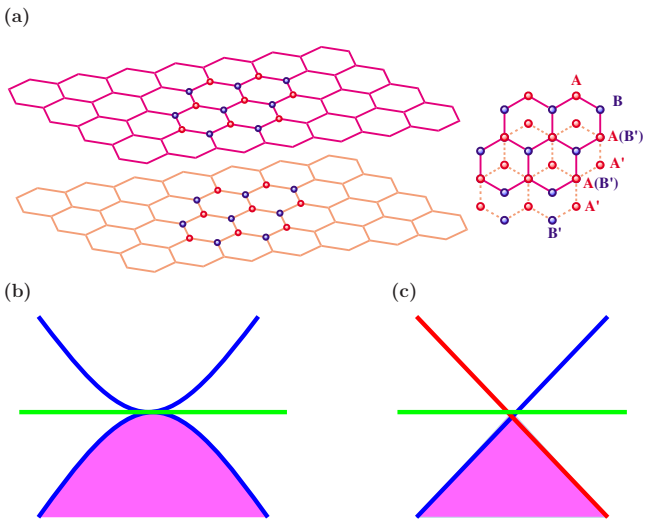

FIG. 1. (Color online) (a) The massive-chiral fermion model describes the low-energy sites in a *AB*-stacked graphene bilayer, those atom sites (top layer *B* sites and bottom layer A' sites) which do not have a neighbor in the opposite layer. (b) The conduction and valence bands of a graphene bilayer touch at the Brillouin-zone corner wave vectors, taken as zero momentum in continuum model theories, and separate quadratically with increasing wave vector. (c) In a 1DES left and right-going electrons cross the Fermi energy at a single point; The momentum of right-going (left-going) electrons is plotted relative to k_F ($-k_F$) where k_F is the Fermi wave vector.

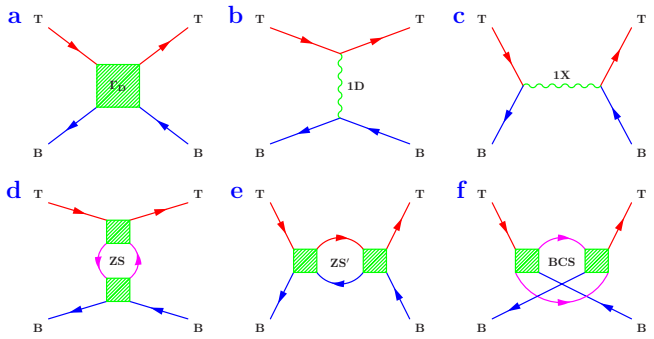

FIG. 2. (Color online) (a) The renormalized interaction Γ_D. (b) and (c) The direct and exchange bare interactions. (d)–(f) They are the one-loop diagrams labeled ZS, ZS′, and BCS, respectively. The external and internal Green's function labels refer to layer in the case of graphene and to chirality in 1DES' case.

cases the Fermi sea is pointlike and there is a gap between occupied and empty free-particle states which grows with wave vector, linearly in the 1DES case. These circumstances are known to support a mean-field broken-symmetry state in which phase coherence is established between conduction and valence-band states for arbitrarily weak repulsive interactions. In the case of a 1DES, the broken-symmetry state corresponds physically to a charge-density-wave (CDW) state, while in the case of bilayer graphene[5] it corresponds to state in which charge is spontaneously transferred between layers. This mean-field-theory prediction is famously incorrect in the 1DES case, and the origin of the failure can be elegantly identified[8,9] using a perturbative renormalization-group (PRG) approach. We show below that when applied to bilayer graphene, the same considerations lead to a different conclusion.

The reliability of the mean-field-theory prediction[5] of a weak-interaction instability in bilayer graphene can be systematically assessed using PRG.[8] We outline the main steps in the application of PRG to bilayer graphene, pointing out essential differences compared to the 1DES case. We assume short-range interactions[10] between electrons in the same (S) and different (D) layers.

The PRG analysis centers on the four-point scattering function defined in terms of Feynman diagrams in Fig. 2. Since the Pauli exclusion principle implies that (in the spinless valleyless case) no pair of electrons can share the same 2D position unless they are in opposite layers, intralayer interactions cannot influence the particles; there is therefore only one type of interaction generated by the RG flow, interactions between electrons in opposite layers with the renormalized coupling parameter Γ_D. The direct and exchange first-order processes in Fig. 2 have the values V_D (bare coupling parameter) and 0, respectively.

The PRG analysis determines how V_D is renormalized in a RG procedure in which high-energy degrees of freedom are integrated out and the fermion fields of the low-energy degrees of freedom are rescaled to leave the free-particle action invariant. The effective interaction Γ_D is altered by coupling between low and high-energy degrees of freedom. At one-loop level this interaction is described[8] by the three higher order diagrams labeled ZS, ZS′, and BCS in Fig. 2. The internal loops in these diagrams are summed over the high-energy labels. In the case of 1DES the ZS loop vanishes and the ZS′ and BCS diagrams cancel, implying that the interaction strengths do not flow to large values and that neither the CDW repulsive interaction nor the BCS attractive interaction instabilities predicted by mean-field theory survive the quantum fluctuations they neglect. The key message of this Rapid Communication is summarized by two observations about the properties of these one-loop diagrams in the bilayer graphene case: (i) the particle-particle (BCS) and particle-hole (ZS and ZS′) loops have the same logarithmic divergences as in the 1DES case in spite of the larger space dimension and (ii) the ZS loop, which vanishes in the 1DES case, is finite in the bilayer graphene case and the BCS loop vanishes instead. Both of these changes are due to a layer pseudospin triplet contribution to the single-particle Green's function as we explain below. The net result is that interactions flow to strong coupling even more strongly than in the mean-field approximation. The following paragraphs outline key steps in the calculations which support these conclusions.

An elementary calculation shows that the single-particle Matsubara Green's function corresponding to the Hamiltonian in Eq. (1) is

$$\mathcal{G}(\boldsymbol{k},i\omega_n)=\begin{pmatrix}\mathcal{G}_{\rm s}(\boldsymbol{k},i\omega_n) & -\mathcal{G}_{\rm t}(\boldsymbol{k},i\omega_n)e^{-iJ\phi_{\boldsymbol{k}}}\\ -\mathcal{G}_{\rm t}(\boldsymbol{k},i\omega_n)e^{iJ\phi_{\boldsymbol{k}}} & \mathcal{G}_{\rm s}(\boldsymbol{k},i\omega_n)\end{pmatrix} \quad (2)$$

where $\hbar\omega_{\boldsymbol{k}}=\xi_{\boldsymbol{k}}=\hbar k^2/2m^*$ and

$$\mathcal{G}_{\rm s,t}(\boldsymbol{k},i\omega_n)\equiv\frac{1}{2}\left(\frac{1}{i\omega_n-\omega_{\boldsymbol{k}}}\pm\frac{1}{i\omega_n+\omega_{\boldsymbol{k}}}\right). \quad (3)$$

The pseudospin-singlet component of the Green's function $\mathcal{G}_{\rm s}$, which is diagonal in layer index, changes sign under frequency inversion whereas the triplet component $\mathcal{G}_{\rm t}$, which is off-diagonal, is invariant.

The loop diagrams are evaluated by summing the product of two Green's functions (corresponding to the two arms of the Feynman diagram loops) over momentum and frequency. The frequency sums are standard and yield ($\beta=(k_{\rm B}T)^{-1}$),

$$\frac{1}{\beta\hbar^2}\sum_{\omega_n}\mathcal{G}^2_{\rm s,t}(i\omega_n)=\mp\frac{\tanh(\beta\xi_{\boldsymbol{k}}/2)}{4\xi_{\boldsymbol{k}}}\underset{T\to 0}{\to}\mp\frac{1}{4\xi_{\boldsymbol{k}}},$$

$$\frac{1}{\beta\hbar^2}\sum_{\omega_n}\mathcal{G}_{\rm s}(i\omega_n)\mathcal{G}_{\rm t}(i\omega_n)\underset{T\to 0}{\to}0, \quad (4)$$

where $\boldsymbol{k}$ is the momentum label shared by the Green's functions. Note that the singlet-triplet product sum vanishes in the low-temperature limit in which we are interested. Each loop diagram is multiplied by appropriate interaction constants (discussed below) and then integrated over high-energy-momentum labels up to the massive-chiral fermion model's ultraviolet cutoff Λ:

$$\int_{\Lambda/s<k<\Lambda}\frac{d^2\boldsymbol{k}}{(2\pi)^2}\frac{\tanh(\beta\xi_{\boldsymbol{k}}/2)}{4\xi_{\boldsymbol{k}}}\underset{T\to 0}{\to}\frac{1}{2}\nu_0\ln(s), \quad (5)$$

where $\nu_0=m^*/2\pi\hbar^2$ is the graphene bilayer density of states. Because $\omega_{\boldsymbol{k}}\propto k^2$, this integral grows logarithmically when the

high-energy cutoff is scaled down by a factor of s in the RG transformation, exactly like the familiar 1DES case. This rather surprising property of bilayer graphene is directly related to its unusual band structure with Fermi points rather than Fermi lines and quadratic rather than linear dispersion.

The key differences between bilayer graphene and the 1DES appear upon identifying the coupling factors which are attached to the loop diagrams. The external legs in the scattering function Feynman diagrams (Fig. 2) are labeled by layer index (T=top layer and B=bottom layer) in bilayer graphene. The corresponding labels for the 1DES are chirality (R=right going and L=left going); we call these interaction labels when we refer to the two cases generically. Since only opposite layer interactions are relevant, all scattering functions have two incoming particles with opposite layer labels and two outgoing particles with opposite layer labels.

In the ZS loop, at the upper vertex the incoming and outgoing T particles induce a B particle-hole pair in the loop while the incoming and outgoing B particles at the lower vertex induce a T particle-hole pair. Since the particle-hole pairs must annihilate each other, there is a contribution only if the single-particle Green's function is off-diagonal in interaction labels. This loop can be thought of as screening V_D; the sign of the screening contribution is opposite to normal, enhancing the bare interlayer interaction, because the polarization loop involves layer pseudospin triplet propagation [see Eq. (4)]. This contribution is absent in the 1DES case because propagation is always diagonal in interaction labels.

The ZS′ channel corresponds to repeated interaction between a T particle and a B hole. This loop diagram involves only particle propagation that is diagonal in interaction labels and its evaluation in the graphene bilayer case therefore closely follows the 1DES calculation. This is the channel responsible for the 1DES mean-field CDW instability in which coherence is established between R and L particles. In both graphene bilayer and 1DES cases it has the effect of enhancing repulsive interactions.

The BCS loop corresponds to repeated interaction between the two incoming particles. In the 1DES case the contribution from this loop which enhances attractive interactions, cancels the ZS′ contribution, leading to marginal interactions and Luttinger liquid behavior. In the graphene bilayer case however, there is an additional BCS loop contribution in which the incoming T and B particles both change interaction labels before the second interaction. This contribution is possible because of the triplet component of the particle propagation and, in light of Eq. (4), gives a BCS loop contribution with a sign opposite to the conventional one. Summing both terms, it follows that the BCS loop contribution is absent in the graphene bilayer case. These results are summarized in Table I and imply that at one-loop level

$$\Gamma_D \simeq \frac{V_D}{1 - V_D \nu_0 \ln(s)}. \tag{6}$$

The interaction strength diverges when $V_D\nu_0 = 1/\ln(s)$, at half[11] the mean-field-theory critical interaction strength. Taking guidance from the mean-field theory,[5] the strong-coupling state is likely a pseudospin ferromagnet which has an energy gap and spontaneous charge transfer between layers.

TABLE I. Summary of contrasting the contributions (in units of the related density of states) of the three one-loop diagrams in 1DES and graphene bilayer cases

Diagrams	ZS	ZS′	BCS	One-loop
1DES	0	$u^2 \ln(s)$	$-u^2 \ln(s)$	0
Graphene bilayer	$\frac{1}{2}\Gamma_D^2 \ln(s)$	$\frac{1}{2}\Gamma_D^2 \ln(s)$	0	$\Gamma_D^2 \ln(s)$

A number of real-world complications have to be recognized in assessing the experimental implications of these results. First of all, electrons in real graphene bilayers carry spin and valley as well as layer pseudospin. This substantially complicates the PRG analysis since many different types of interactions are generated by the RG flow. One simplification is that interactions conserve spin, and both layer and valley pseudospin, at each vertex. Interactions are however dependent on whether the interacting particles are in the same (S) or in different (D) layers. The fermion propagators conserve both spin and valley pseudospin but not the layer pseudospin as shown in Eq. (2). It is immediately clear then that the incoming and outgoing total spin must be preserved for real spin and for the valley pseudospin, and the same conclusion applies for the layer pseudospin after a more elaborate consideration. From Eq. (2) we see that a phase factor $e^{\pm 2i\phi_q}$ is gained when the propagator transfers electrons between layer indices with the + applying for top to bottom evolution and the − for bottom to top. Unless these transfers enter an equal number of times, the integrand in a Feynman diagram will contain a net phase factor related to chirality and vanish under momentum integration. The total layer pseudospin is therefore also conserved in collisions.

When one spin degree of freedom is considered, as in the 1DES case, three types of interactions have to be recognized, Γ_S, Γ_D, and Γ_X. Γ_S couples electrons with the same flavor and Γ_D electrons with different flavors, while Γ_X is the exchange counterpart of Γ_D. The bare value of the exchange part of Γ_D (the direct part of Γ_X) is of course zero since the Coulomb interaction is flavor independent, but higher order contributions are nonzero if triplet electron propagation is allowed. Correspondingly, when both spin and valley degrees of freedom are acknowledged the interaction parameters are Γ_{SSD}, Γ_{SDS}, Γ_{SDD}, Γ_{DSS}, Γ_{DSD}, Γ_{DDS}, Γ_{DDD}, Γ_{XSD}, Γ_{XDS}, and Γ_{XDD}, considering Pauli exclusion principle and the fermionic antisymmetry between outgoing particles. The labels refer from left to right to layer, real spin and valley. The flow of the renormalized interactions is illustrated in Fig. 3 and they diverge near $V_D\nu_0 \simeq 0.6/\ln(s)$. The instability tendency is therefore somewhat enhanced by the spin and the valley degrees of freedom.

Next we must recognize that the massive-chiral fermion model applies only between trigonal-warping and interlayer hopping energy scales. Appropriate values for $\ln(s)$ in the RG flows are therefore at most around $\ln(s)_{\max} = \ln(k_H/k_L) \simeq \ln(\gamma_0/\gamma_3) \simeq 2.3$, using accepted values for the hopping parameters.[1,4] We estimate the strength of the bare scattering amplitudes in vacuum by evaluating the 2D Coulomb scat-

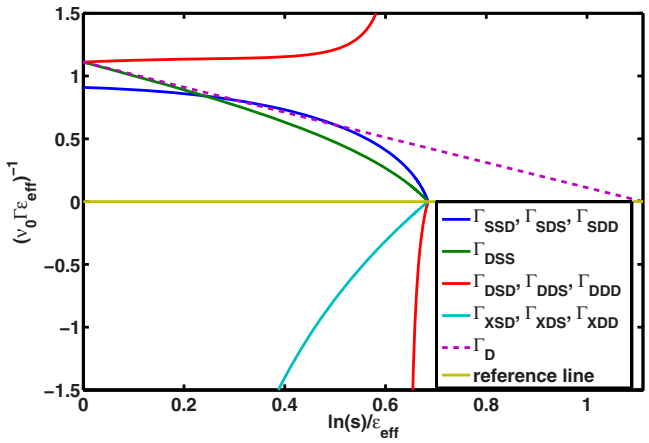

FIG. 3. (Color online) This illustration plots the inverse interaction strength $(\nu_0\Gamma\varepsilon_{\text{eff}})^{-1}$ versus the scaling parameter $\ln(s)/\varepsilon_{\text{eff}}$. ε_{eff} is the effective dielectric constant of the graphene bilayer and $\Gamma=\Gamma_{\text{vacuum}}/\varepsilon_{\text{eff}}$. Interlayer interaction parameters Γ_{DSS} (green) and $\Gamma_{XSD}, \Gamma_{XDS}, \Gamma_{XDD}$ (cyan) flow to large values most quickly. According to this estimate the normal state becomes unstable for $V_D \geq 0.6/\ln(s)$.

tering potential at the high-energy cutoff wave vector $\nu_0 V_S \simeq (m^*/2\pi\hbar^2)(2\pi e^2/k_{\text{H}}) = \alpha_{\text{ee}}/2$, where $\alpha_{\text{ee}} = e^2/\hbar v_{\text{F}} \simeq 2.2$ is graphene's fine-structure constant. The value used for V_D is reduced by a factor of $e^{-k_{\text{H}}d}$ compared to V_S to account for the layer separation $d=3.35$ Å. According to these estimates the bare value of $\nu_0 V_D$ exceeds the stability limit of $\sim 0.6/\ln(s)_{\max} \sim 0.25$ by approximately a factor of four. For graphene layers on the surface of a substrate with dielectric constant ε, interactions are reduced by a factor of $\sim(\varepsilon+1)/2$. In the case of SiO_2 substrates $\varepsilon \sim 4$, the instability still occurs but the interaction strength exceeds the stability limit by a much narrower margin.

Lastly we expect that additional screening effects from graphene σ orbitals, which are normally neglected in continuum model calculations, will reduce interaction strengths at wave vectors near k_{H} somewhat and favor stable bilayers.

Gaps do appear in bilayer graphene even when electron-electron interactions are neglected, provided that an external potential difference V is applied between the layers. The potential adds a single-particle term $-V\tau^z/2$ to the single-particle Hamiltonian, breaks inversion symmetry, and transfers charge[12–15] between layers. This interesting property is the basis of one strategy currently being explored[16,17] in the effort to make useful electronic devices out of graphene 2DESs. Even if gaps do not appear spontaneously in real bilayer graphene samples, it is clear from the present work that interesting many-body physics beyond that captured by commonly used electronic-structure-theory approximations (local-density approximation or generalized gradient approximations, for example), must play at least a quantitative role in determining gap grown with V. As graphene bilayer sample quality improves, we expect that it will be possible to explore this physics experimentally with angle resolved photoemission spectroscopy, tunneling, and transport probes. At this point, we would like to note that three complementary preprints,[18–20] which cover closely related material, have appeared recently.

This work has been supported by the Welch Foundation and by the National Science Foundation under Grant No. DMR-0606489. A.H.M. gratefully acknowledges helpful discussion with R. Shankar and I. Affleck.

[1] T. Ando, J. Phys. Soc. Jpn. **74**, 777 (2005).
[2] A. K. Geim and K. S. Novoselov, Nature Mater. **6**, 183 (2007).
[3] A. K. Geim and A. H. MacDonald, Phys. Today **60**(8), 35 (2007).
[4] A. H. Castro Neto *et al.*, Rev. Mod. Phys. **81**, 109 (2009).
[5] H. Min, G. Borghi, M. Polini, and A. H. MacDonald, Phys. Rev. B **77**, 041407(R) (2008).
[6] E. McCann and V. I. Fal'ko, Phys. Rev. Lett. **96**, 086805 (2006).
[7] Y. Barlas, T. Pereg-Barnea, M. Polini, R. Asgari, and A. H. MacDonald, Phys. Rev. Lett. **98**, 236601 (2007).
[8] R. Shankar, Rev. Mod. Phys. **66**, 129 (1994).
[9] T. Giamarchi, *Quantum Physics in One Dimension* (Clarendon Press, Oxford, 2003).
[10] We replace the bare Coulomb interactions by short-range momentum-independent interactions (Ref. 8) by evaluating them at typical momentum transfers at the model's high-energy limit. We believe that this approximation is not serious because of screening.
[11] Mean-field theory is equivalent to a single-loop PRG calculation in which only one particle-hole channel is retained. For the drawing conventions of Fig. 2 the susceptibility which diverges at the pseudospin ferromagnet phase boundary is obtained by closing the scattering function with τ^z vertices at top and bottom, so the appropriate particle-hole channel is the ZS channel not the ZS′ channel.
[12] T. Ohta *et al.*, Science **313**, 951 (2006).
[13] E. V. Castro, K. S. Novoselov, S. V. Morozov, N. M. R. Peres, J. M. B. Lopes dos Santos, J. Nilsson, F. Guinea, A. K. Geim, and A. H. Castro Neto, Phys. Rev. Lett. **99**, 216802 (2007).
[14] E. McCann, Phys. Rev. B **74**, 161403(R) (2006).
[15] H. Min, B. Sahu, S. K. Banerjee, and A. H. MacDonald, Phys. Rev. B **75**, 155115 (2007).
[16] J. B. Oostinga *et al.*, Nature Mater. **7**, 151 (2008).
[17] J. Martin, Bull. Am. Phys. Soc. **54**, 191 (2009).
[18] O. Vafek and K. Yang, Phys. Rev. B **81**, 041401 (2010).
[19] K. Sun, H. Yao, E. Fradkin, and S. Kivelson, Phys. Rev. Lett. **103**, 046811 (2009).
[20] R. Nandkishore and L. Levitov, arXiv:0907.5395 (unpublished).